PNAS RESEARCH ARTICLE | NEUROSCIENCE OPEN ACCESS

Principles of nociceptive coding in the anterior cingulate cortex

Mario A. Acuña[a,1], Fernando Kasanetz[a,b,1], Paolo De Luna[a], Marta Falkowska[a], and Thomas Nevian[a,2]

Edited by Allan Basbaum, University of California San Francisco, San Francisco, CA; received July 24, 2022; accepted April 26, 2023

The perception of pain is a multidimensional sensory and emotional/affective experience arising from distributed brain activity. However, the involved brain regions are not specific for pain. Thus, how the cortex distinguishes nociception from other aversive and salient sensory stimuli remains elusive. Additionally, the resulting consequences of chronic neuropathic pain on sensory processing have not been characterized. Using in vivo miniscope calcium imaging with cellular resolution in freely moving mice, we elucidated the principles of nociceptive and sensory coding in the anterior cingulate cortex, a region essential for pain processing. We found that population activity, not single-cell responses, allowed discriminating noxious from other sensory stimuli, ruling out the existence of nociception-specific neurons. Additionally, single-cell stimulus selectivity was highly dynamic over time, but stimulus representation at the population level remained stable. Peripheral nerve injury-induced chronic neuropathic pain led to dysfunctional encoding of sensory events by exacerbation of responses to innocuous stimuli and impairment of pattern separation and stimulus classification, which were restored by analgesic treatment. These findings provide a novel interpretation for altered cortical sensory processing in chronic neuropathic pain and give insights into the effects of systemic analgesic treatment in the cortex.

neuropathic pain | anterior cingulate cortex | in vivo calcium imaging | sensory representation | nociception

Significance

Our work elucidates fundamental principles of nociceptive and sensory coding in the anterior cingulate cortex (ACC). Specifically, 1) Discrimination of nociceptive from other sensory stimuli in the ACC depends on population coding. 2) Single-cell stimulus representation is dynamic over time. 3) There are no nociception-specific neurons in the ACC. 4) Nociception can be regarded as a special case of sensory detection. 5) Chronification of pain leads to an impairment of the decoding accuracy of sensory information, resulting in a misinterpretation of innocuous stimuli as noxious. 6) Analgesia induces a normalization of neuronal network function in the ACC. Therefore, our work contributes to the understanding of the complexity of cortical nociceptive and sensory processing and its alteration in chronic neuropathic pain.

The perception of pain is a complex phenomenon that requires activity in distributed regions of the brain. However, it is still largely unclear how a noxious stimulus is processed in cortical brain regions and which patterns of activity make nociception distinct from other salient sensory events. Functional brain imaging in humans identified several brain areas activated by noxious stimuli, which together represent the different aspects of the pain experience (1). Nevertheless, the activity in the so-called pain matrix is not specific for pain. The comprising brain regions are involved in multiple and diverse processes other than pain and similar responses in the pain matrix can be elicited by salient but nonpainful sensory stimuli (2, 3). Despite this, nociception and the resulting experience of pain must be reliably encoded by specific activity patterns across and within regions of the pain matrix (4). Such nociception-specific responses could stem from dedicated "pain" neurons together with the activity of a broader multifaceted neuronal network. How exactly such neuronal ensembles within each cortical area of the pain matrix code for nociception is largely unknown, however important for a comprehensive understanding of the pain experience.

The anterior cingulate cortex (ACC) is an essential brain area participating in the affective and emotional connotation of pain. The human ACC is not only reliably activated by noxious stimuli, but also the magnitude of the nociceptive response correlates with stimulus intensity and discomfort (5–7). Furthermore, patients with lesions in the ACC report altered emotional pain perception (8). In rodents, manipulations that reduce or eliminate ACC activity show impaired affective behavior to noxious stimuli (9–12). However, the neuronal mechanisms by which ACC neurons encode the aversive quality of nociceptive sensory stimuli and distinguish them from other aversive, salient, or neutral events have not yet been characterized. While in vivo acute and chronic electrophysiological recordings in the ACC have identified neuronal responses to noxious stimuli (12–15), their specificity for nociception over other sensory modalities remains unclear. Just as it is currently unresolved whether nociceptive coding in the ACC is a matter of single neuron representations or of coordinated neuronal ensembles.

Patients suffering from chronic pain show elevated stimulus-evoked activations in the ACC associated with increased unpleasantness (1, 16–18). In rodents, we and others have shown that the transition to chronic pain is characterized by changes in the ACC based on neuronal plasticity (19–23). The overall nature of the reported changes points toward an increased excitability, modified connectivity and altered activity within the neuronal network. However, it is elusive how these plastic changes may affect sensory-coding capabilities of the ACC in vivo.

Author affiliations: [a]Department of Physiology, University of Bern, Bern 3012, Switzerland; and [b]Grupo de Neurociencia de Sistemas, Instituto de Fisiología y Biofísica "Bernardo Houssay", Universidad de Buenos Aires y Consejo Nacional de Investigaciones Científicas y Técnicas, Grupo de Neurociencia de Sistemas, Buenos Aires C1121ABG, Argentina

Author contributions: M.A.A., F.K., and T.N. designed research; M.A.A., F.K., and M.F. performed research; P.D.L. contributed new reagents/analytic tools; M.A.A., F.K., P.D.L., M.F., and T.N. analyzed data; and M.A.A., F.K., and T.N. wrote the paper.

The authors declare no competing interest.

This article is a PNAS Direct Submission.

[1]M.A.A. and F.K. contributed equally to this work.

[2]To whom correspondence may be addressed. Email: thomas.nevian@unibe.ch.

This article contains supporting information online at https://www.pnas.org/lookup/suppl/doi:10.1073/pnas.2212394120/-/DCSupplemental.

Published May 30, 2023.

In this study, we investigated the neuronal network dynamics in the ACC in freely moving mice using fluorescent calcium imaging, which allowed us to compare the neuronal activity evoked by a number of different sensory stimuli, ranging from neutral over aversive to nociceptive. The analysis of the activity patterns revealed the coding capability of the ACC. Repeated imaging of the same neurons in multiple sessions gave insight into the question of stability of the sensory representation over time. In addition, we examined the changes of the activity patterns and sensory representation in chronic neuropathic pain and how they could be affected by the widely used analgesic drug gabapentin (GBP). Overall, we found that nociceptive processing in the ACC depended on population coding rather than on nociception-specific neurons and that the sensory representation was highly dynamic over time. Chronic neuropathic pain leads to a misclassification of sensory stimuli, a loss of mutual information and a detrimental rearrangement in the connectivity. Some of these network changes were restored by GBP. Thus, these findings allow a novel interpretation of chronic neuropathic pain and its analgesic treatment as a network phenomenon.

Results

Stimulus Representation in the ACC of Freely Moving Mice. We imaged ACC neuronal activity in vivo to understand how nociception is encoded and distinguished from other sensory stimuli. We took advantage of gradient-index (GRIN) lenses to directly image from ventral ACC deep-layer pyramidal neurons (24) using the genetically encoded calcium-indicator GCaMP6f under the calcium/calmodulin-dependent protein kinase II (CaMKII) promotor, that otherwise were not in range for conventional cranial window imaging (25) (Fig. 1 *A* and *B* and see *SI Appendix*, Fig. S1 for a detailed reconstruction of the imaging locations). Freely moving animals carrying a miniaturized microendoscope (miniscope) were presented with a battery of innocuous, aversive and noxious stimuli while the neuronal population dynamics were measured (Fig. 1 *A* and *C* and *SI Appendix*, Fig. S2 *A* and *B*). Noxious cold, heat, pinprick (representing noxious stimuli), air puff to the face (an aversive, but non-noxious stimulus) and dynamic touch (salient as the others, but a neutral non-noxious stimulus) elicited distinct patterns of activity and activated specific neuronal ensembles. Characterizing the single-cell activity in terms of stimulus encoding, we found that from a total of 698 neurons (69.8 ± 4.47 neurons per animal), sensory stimuli elicited significant calcium responses in ~48% of imaged ACC neurons, with ~77% of responses being activations and 23% inhibitions with an average response reliability for each stimulus of ~25% (*SI Appendix*, Figs. S2*C* and S3 *A–C*). From all cells, 34% were unimodal, i.e., responded to only one stimulus, while a set of 14% were multimodal neurons that may carry information about common features across different stimuli. When compared to simulated data, we observed a higher-than-expected proportion of multimodal neurons and a lower-than-expected proportion of unimodal neurons (Fig. 1*D*), demonstrating a nonrandom architecture of the neural network of the ACC modulated by sensory stimuli. Multimodal neurons showed mixed responses of a varying degree to the sensory stimuli (Fig. 1*F*). The biggest class were supramodal cells that responded both to noxious and non-noxious stimuli (9.6% of cells) and putative nociceptive cells that responded exclusively to two or more noxious stimuli (4.1%; Fig. 1 *E* and *F*). Nevertheless, whereas the supramodal cells were observed more often than expected by chance, the number of neurons responding to noxious stimuli only was not different from chance level (Fig. 1*E*), suggesting that there was no significant nociception-specific ensemble in the ACC that solely reacted to a common feature of the nociceptive stimuli. Additionally, noxious stimuli activated supramodal neurons to an equal degree as compared to the spurious nociceptive ensemble (Fig. 1*G*). Comparing the average evoked activity of the stimulus selective neurons for different stimuli revealed a graded response depending on stimulus strength. Noxious cold and pinprick applied to the left hindpaw led to a stronger activation as compared to touch (Fig. 1*H*). Altogether, this suggests that specific neuronal ensembles in the ACC were efficiently activated by sensory stimuli, a portion of which may encode generalized features of the stimulus (i.e., concepts), which might help generating high-level sensory percepts. Nevertheless, our results rule out the contribution of a nociception-specific ensemble in the ACC, and suggest that nociceptive encoding is achieved by the activity of a population of neurons that encompasses stimulus-selective and supramodal ensembles. Yet, the stimulus-selective neurons could form specific ensembles that represent the different qualities of the nociceptive stimuli (i.e., burning or stabbing).

Accordingly, we found that the population activity in the ACC reliably and robustly discriminated between stimuli (Fig. 1 *I* and *K*). Removing the unimodal cells from the decoding procedure gave equally good decoding as removing the same number of random cells (*SI Appendix*, Fig. S4). This efficient classification was partly a result of an effective separation of stimulus responses within the neuronal population (Fig. 1*L*). Overall, these results provide evidence for a robust representation of sensory stimuli by characteristic activity patterns of the neuronal population in the ACC and not depending on the activity of single cells.

Stability of Stimulus Representation Over Time. The encoding of stimulus features in individual neurons is generally stable over time in primary sensory cortices (25–30). However, stimulus representation on the cellular level tends to continuously reconfigure in associative areas, despite stable behavioral performance (30–32). It is currently unclear how the temporal dynamics of nociceptive representation in higher cortical areas evolve over time at the cellular level (33). Resolving this question will help to understand if sensory representation and particularly nociception and its quality-specificity are achieved through hard-wired, stable and dedicated neurons or by flexible and dynamic neuronal ensembles. We therefore evaluated the neuronal representational changes over time in up to three consecutive sessions separated by 7 d in naïve freely moving, awake animals (Fig. 2*A*). Across sessions, the amplitude and frequency of the spontaneous calcium events of individual neurons were significantly correlated (*SI Appendix*, Fig. S5 *A* and *B*). Moreover, the population average of the spontaneous calcium event amplitudes and frequencies was conserved (*SI Appendix*, Fig. S5*B*).

Evoked responses to the different stimuli were highly variable from one session to another, showing considerable reconfiguration of single-cell tuning (Fig. 2 *A* and *C*). We identified neurons that gained responsiveness, neurons that lost responsiveness, neurons that remained stable, and neurons that changed the sign of responsiveness from being activated to being inhibited or vice versa (swap neurons) (Fig. 2*D*). Even though a large portion of neurons changed their stimulus identity, the total number of neurons in a stimulus ensemble remained constant, as there was an apparent homeostatic balance of equal proportion of neurons gaining and losing selectivity (Fig. 2 *D* and *E* and *SI Appendix*, Fig. S5 *C* and *D*). Next, we assessed the stability of responsiveness (i.e., an intrinsic value that characterizes the degree at which a neuron is detected as responsive) and reliability (i.e., the proportion of trials in which a stimulus response was detected to be significant), two attributes

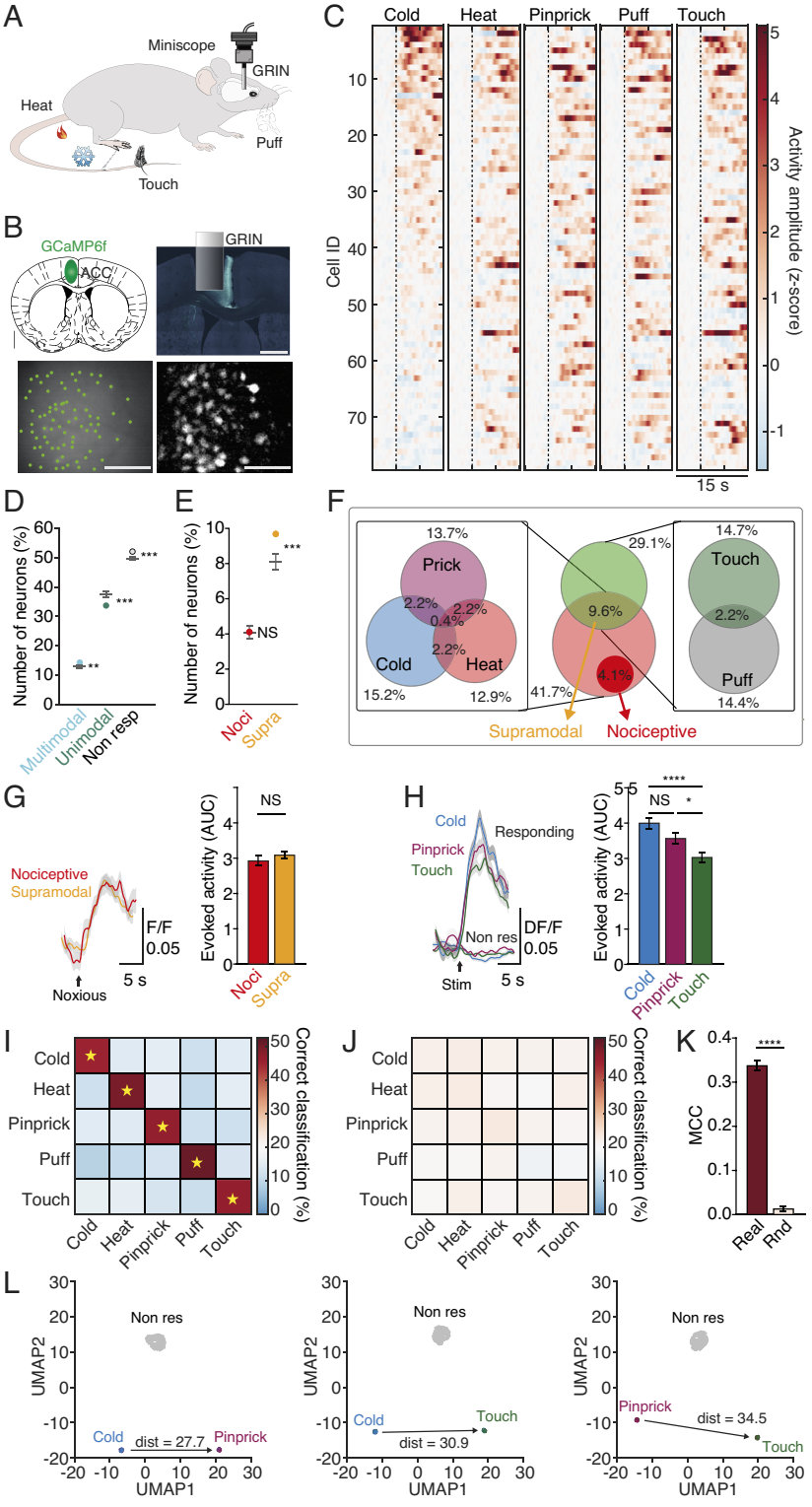

Fig. 1. Sensory stimulus representation in the ACC. (*A*) Schematic of the experimental paradigm. Freely moving mice carrying a miniature microscope (miniscope) and expressing the calcium indicator GCaMP6f under the CamKII promoter (ssAAV1/2.mCaMKIIa.GCaMP6f.WPRE.SV40(A); mCaMKIIa-1288) in the ACC were presented with a battery of noxious (dry ice cold, pinprick, heat), aversive (air puff) and innocuous (dynamic brush touch) stimuli. (*B*, *Top*) schematic of GCaMP6f expression (*Left*) and histological brain slice illustrating GRIN lens placement in the ACC (*Right*); (scale bars, 1 mm.) (*Bottom*) map of active neurons derived from raw miniscope images (*Left*) and mean correlation of active ACC neurons (*Right*); (scale bars, 100 µm.) (*C*) Heatmap showing mean activity over time (z-scored ΔF/F) for the presented stimuli across all trials from a single session corresponding to the FOV shown in *B*. Neurons were aligned to their maximal response evoked by cold. Individual neuron identities are consistent across stimuli. (*D*) Percentage of unimodal (responding to only one stimulus), multimodal (responding to two or more stimuli) and nonresponsive neurons based on logistic regression selectivity classification. Gray lines (mean ± SD) represent the chance distribution obtained from 1,000 simulated sessions. Circles are the experimentally observed values. ***P < 0.001, **P < 0.01 based on z-score values. (*E*) Percentage of supramodal (neurons with significant responses to noxious and non-noxious stimuli) and nociceptive (neurons with significant responses to exclusively two or more noxious stimuli and no responses to non-noxious stimuli) from all neurons analyzed in the naïve condition. Gray lines (mean ± SD) represent the chance distribution obtained from 1,000 simulated sessions. Circles are the experimentally observed values. ***P < 0.001, ns P > 0.05 based on z-score values. (*F*) Venn diagram of proportions of neurons responding to the different sensory stimuli and the definition of nociceptive and supramodal ensembles. (*G*) Noxious stimulus-evoked average neuronal activity within the supramodal and the spurious nociceptive ensemble. (*Left*) stimulus-evoked mean Ca^{2+} transients. Mean, solid line; shaded area, ± SEM. (*Bottom*) quantification of stimulus-evoked responses (AUC). ns P > 0.05, unpaired t test. Supramodal, n = 6,386 trials, 2,108 neurons; nociceptive, n = 2,703 trials, 903 neurons. (Scale bars, 0.05 ΔF/F, 5 s.) (*H*) Stimulus-evoked average neuronal activity within stimulus selective ensembles (i.e., neurons with significant responses to the stimulus). (*Left*) stimulus-evoked mean Ca^{2+} transients for the responsive ensembles and the corresponding signals in the nonresponding cells as reference. Mean, solid line; shaded area, ± SEM. (*Right*) quantification of stimulus-evoked responses (AUC). One-way ANOVA, F(2, 10,264) = 12.3. Post hoc Bonferroni correction, *P < 0.05, ***P < 0.001, ns P > 0.05. Cold, n = 3,567; pinprick, n = 3,284; touch, n = 3,416 trials. (*I*) Stimulus classification of a multiclass linear discriminant classifier that distinguishes the population activity pattern for noxious cold, heat, pinprick, puff, and touch. The values on-diagonal (actual stimulus) were compared to all off-diagonals (incorrect stimuli) and normalized to 100%. Yellow stars indicate correct classification (P < 0.05) of the actual stimulus over off-diagonal stimuli within the same row (Wilcoxon signed-rank). (*J*) Same as (*I*) but labels were shuffled. (*K*) Quantification of stimulus classification by Matthew's correlation coefficient. Significant correct classification for observed data against random labels. ****P < 0.0001. Paired t test, n = 38 sessions, 10 animals. (*L*) Clustering of neurons (dots) based on the post-stimulus response classification based on logistic regression analysis using UMAP. (*Left*) comparison between pinprick and cold. (*Middle*) comparison between touch and cold. (*Right*) comparison between pinprick and touch. After k-means clustering, Euclidean distances between centroids are depicted. Data is pooled across 30 naïve sessions for 10 animals.

which carry information about the quality of the stimulus representation. We compared the magnitude of gained vs. lost responsiveness and reliability across sessions. For all the evaluated stimuli, neither of the two parameters changed (*SI Appendix*, Fig. S5*D*). Thus, sensory stimulus representation at the population level remained stable in quantity (proportion) and quality (responsiveness and reliability). In this way, the brain can achieve stability with a high degree of flexibility (31).

We next examined the temporal stability of neuronal ensembles between two consecutive sessions. First, we observed that the proportion of supramodal neurons remained constant over time (Fig. 2 *F* and *G*). Moreover, the stimulus-evoked activity within this supramodal ensemble was also stable (*SI Appendix*, Fig. S5*E*). Additionally, we found a representation above chance levels for the supramodal ensemble that was stable over time, while the spurious nociceptive neurons remained at chance level (Fig. 2*H*). We further found a significant proportion of neurons (1.7%) that kept their corresponding supramodality over time (Fig. 2*I*). Thus, our data identified a subset of ACC neurons showing perdurable specificity for sensory representation, but not for nociception. This, together

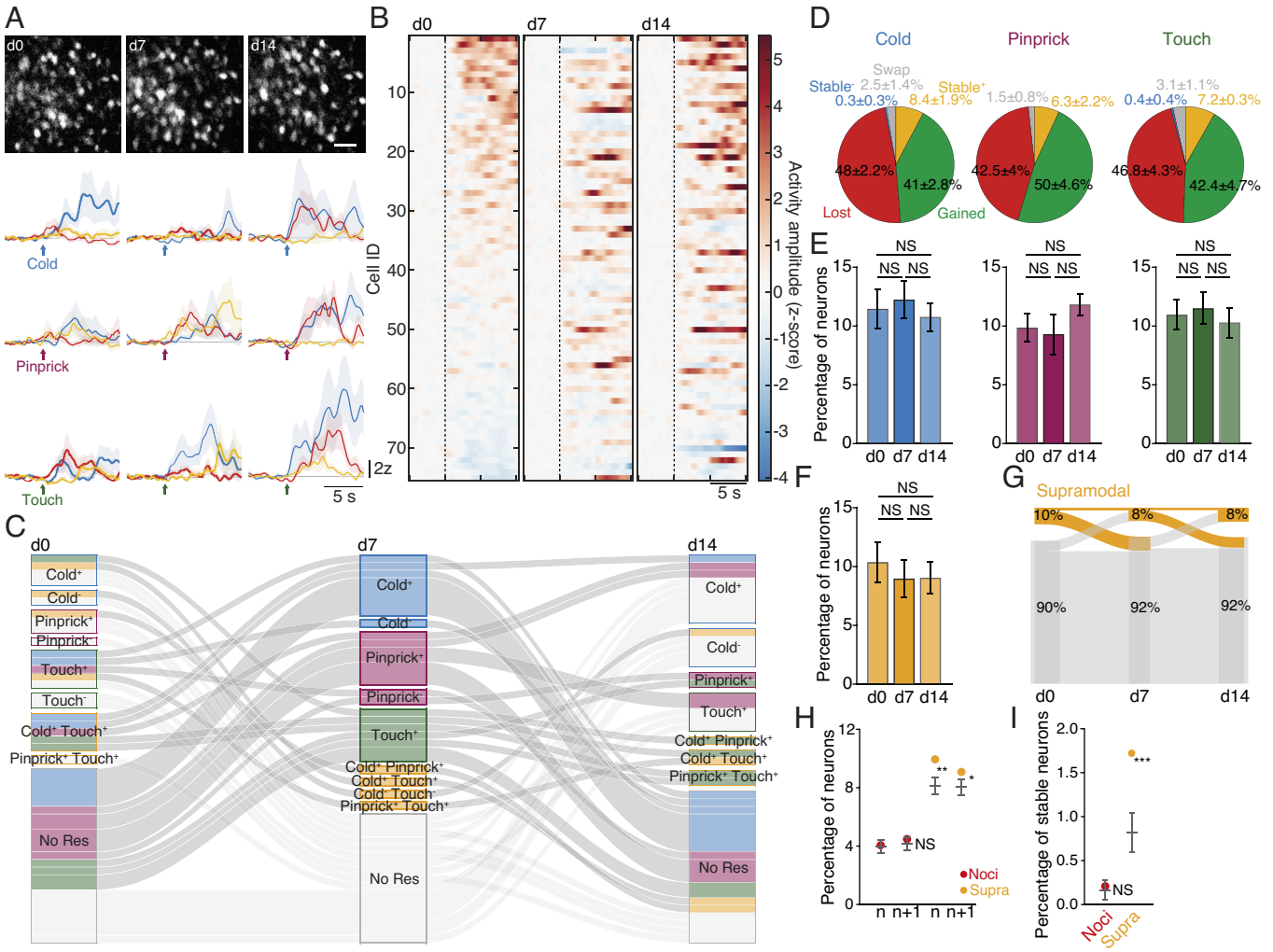

Fig. 2. Temporal stability of stimulus representation in the ACC. (*A*) Correlation maps of active neurons derived from mean correlation of pixels across 3 consecutive sessions. Note the high similarity of the three FOVs. (Scale bar, 100 μm.) (*Bottom*) fluorescent traces (z-scored) illustrating the stimulus-evoked activity from three neurons (red, blue and orange) to cold, pinprick and touch in three consecutive sessions. Arrows indicate the time of stimulus presentation. (*B*) Heatmap depicting the mean Ca^{2+} activity (z-scored ΔF/F) over time for noxious cold across three consecutive sessions, separated by 7 d, sorted to the neuron with the highest stimulus-evoked activity in session one. (*C*) Alluvial plot illustrating the change in neuronal responsiveness over sessions for cold, pinprick and touch from one example animal. "None" indicates a population of neurons that was classified as nonresponsive to either stimulus. Each individual line represents a single neuron tracked over time. (+) indicates positively modulated neurons and (−) denotes negatively modulated neurons by the respective stimulus. Neurons were ordered and color-coded according to their stimulus selectivity in the second session. (*D*) Pie charts depicting the proportion of neurons that either gained, lost, reversed responses (swap; from inhibited to activated, or vice versa), or remained stable across sessions for cold, heat and touch (mean percent ± SEM). (*E*) Quantification of proportion of selective cells across sessions for cold, pinprick and touch. The lack of significant differences points towards stability of the sensory representation by selective neurons over time. One-way repeated measures ANOVA [cold: F(1.938, 17.45) = 0.43, pinprick: F(1.429, 12.86) = 0.9610, touch: F (1.666, 15.00) = 0.3280] Tukey correction, "ns", $P > 0.05$. (*F*) Percentage of neurons in the supramodal ensemble across sessions. One-way repeated measures ANOVA, F(1.770, 15.93) = 0.7829, Tukey correction, ns, $P > 0.05$. (*G*) Illustration of the evolution of the supramodal ensemble over time from pooled data of all animals and sessions (n = 2,094 neurons). (*H*) Percentage of neurons belonging to the spurious nociceptive or supramodal ensemble in two successive sessions (n and n+1). Gray lines (mean ± SD) represent the chance distribution and circles are the experimentally observed values. ***$P < 0.001$, **$P < 0.01$, *$P < 0.05$ from chance based on z-scores. (*I*) Percentage of neurons that maintain ensemble-specificity in two successive sessions. Gray lines (mean ± SD) represent the chance distribution and circles are the experimentally observed values. ***$P < 0.001$ based on Z scores.

with the stable population encoding capabilities, may provide the ACC with the ability to keep sensory encoding constant in the presence of continuous change of single-neuron representation (31, 34).

Network Changes after the Transition to Neuropathic Pain. ACC neuronal circuits undergo substantial synaptic and intrinsic modifications during the development of neuropathic pain (19–22), which are believed to play a central role in its symptomatology. However, the consequences of the described cellular changes on the circuit dynamics are still elusive. Therefore, we investigated how sensory representation and its neuronal dynamics were affected in neuropathic pain using the spared nerve injury (SNI) model in animals implanted with GRIN lenses (Fig. 3*A*). In neuropathic animals, we observed an increase in mechanical sensitivity (Fig. 3*B*) and a significant increase in the proportion of affective/motivational behavioral responses to sensory stimuli that were nearly absent in naïve and sham mice (Fig. 3*C* and *SI Appendix*, Fig. S6 *A* and *B*). The stimulus-evoked neuronal activity patterns recorded in the ACC allowed efficient decoding of the corresponding behavior of the animals (Fig. 3*D*). This could partially be explained by a differentially evoked activity observed in the stimulus-selective ensemble (*SI Appendix*, Fig. S6 *C* and *D*). These results suggest that the ACC is contributing to the transformation of sensory stimuli into an adequate behavioral response in the chronic pain condition.

Nerve injury resulted in increased spontaneous neuronal activity in the ACC (Fig. 3 *E* and *F*). When looking at distinct neuronal ensembles, we observed that neurons belonging to the supramodal

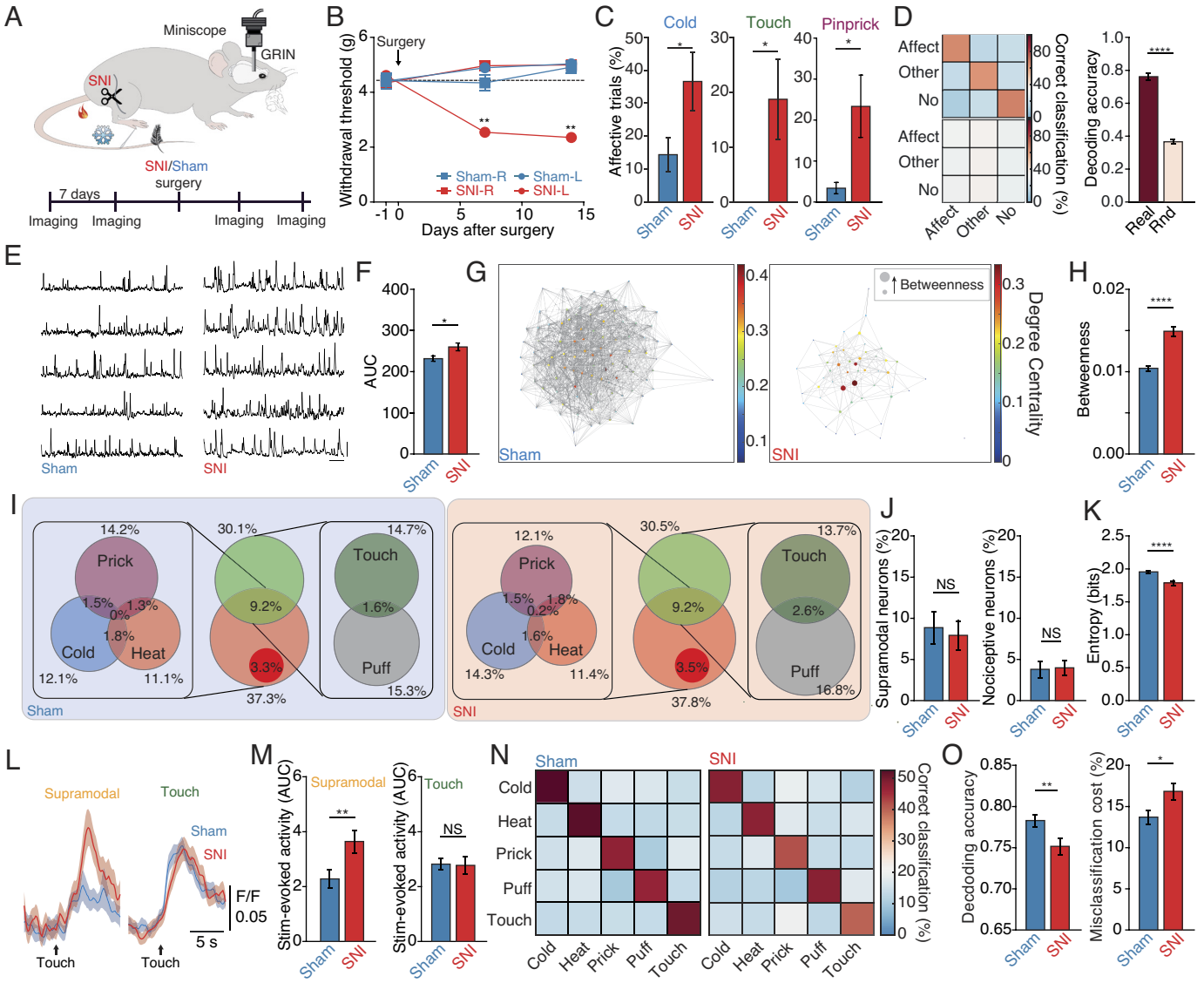

Fig. 3. Neuropathic pain impairs sensory coding in the ACC. (*A*) Schematic of the experimental procedure to evaluate neuronal changes after the induction of neuropathic pain by SNI. (*B*) Mechanical sensitization evaluated by the electronic Von Frey test. Animals were subjected to either sham (n = 5, blue circles) or SNI (n = 5, red circles) surgery of the left hind paw. Von Frey tests were performed 1 d before and +7 and +14 d after surgery. Two-way repeated measures ANOVA, interaction time × surgery: F(6, 36) = 17.27, Bonferroni post hoc test, $^{**}P < 0.01$, after surgery vs. before surgery. Dashed line indicates average mechanical threshold for paw withdrawal before surgery. (*C*) Percentage of trials, in which animals showed stimulus-evoked affective/motivational responses to cold, touch, and pinprick (14 sessions each), $^{*}P < 0.05$, unpaired *t* test. (*D*) Linear discriminant classification of neuronal activity patterns correlated to two categories of behavior in neuropathic animals. The first behavior were affective/motivational, temporally delayed responses, in which the animal engaged into directed licking and biting of the paw, paw extended lift or guarding, and/or escape responses characterized by hyperlocomotion, rearing, or jumping away from the noxious or non-noxious stimulus ("Affect"). The second behavior ("Other") was a stimulus-dependent, attentional shift, in which the mice responded by shifting the attention to the stimulus without expressing affective/motivational behaviors. No behavior ("No") refers to trials in which the animals did not show any complex behavior. (*Left*) *Top*, observed classification values; *Bottom*, shuffled labels. (*Right*) accuracy of decoding expressed as MCC (n = 10 sessions), paired *t* test, $^{****}P < 0.0001$. (*E*) Example recordings of Ca^{2+} transients, depicting the increase of activity in the resting state (spontaneous) neuronal activity in the SNI group. (Scale bars, ΔF/F 0.01, 60 s.) (*F*) Quantification of the integral of Ca^{2+} transients during 10 min recordings of spontaneous activity. $^{*}P < 0.05$, unpaired *t* test. Sham, n = 728; SNI, n = 539 neurons. (*G*) Graph-theoretic functional connectivity analysis of spontaneous neuronal calcium activity in the ACC. Representative graph plots depicting the neuronal network from a sham and a SNI animal. Circle size indicates level of betweenness centrality (*Inset*). Colors indicate levels of degree centrality. (*H*) Bar plot of normalized betweenness centrality of undirected graph analysis from the adjacency matrix of cross-correlated activity. Data was pooled across animals and sessions $^{****}P < 0.0001$, unpaired *t* test. Sham, n = 1,173; SNI, n = 846 neurons. (*I*) Venn diagram of proportions of neurons responding to the different sensory stimuli for sham and SNI animals. (*J*, *Left*) proportion of supramodal neurons in sham and SNI animals. NS, $P > 0.05$, unpaired *t* test. (*Right*) proportion of nociceptive neurons in sham and NP. NS $P > 0.05$, unpaired *t* test. Sham, n = 9 sessions; NP, n = 9 sessions. (*K*) Bar graph of entropy values, measured as Shannon's Entropy bits, in sham and SNI conditions during resting state activity. $^{****}P < 0.0001$, unpaired *t* test. Sham, n = 390; SNI, n = 307 neurons. (*L*) Touch elicits increased activity within the supramodal ensemble, but not within the selective ensemble. Stimulus-evoked mean Ca^{2+} transients for touch in neurons within the supramodal (*Left*) and the touch-selective (*Right*) ensemble. Mean, solid line; shaded area, ± SEM. (*M*) Average touch-evoked activity (mean ± SEM), $^{**}P < 0.01$, unpaired *t* test. Sham, n = 509; SNI, n = 460 neurons within the supramodal ensemble (*Left*). NS, $P > 0.05$, unpaired *t* test. Sham, n = 315; SNI, n = 399 neurons within the selective ensemble (*Right*). (*N*) Confusion matrix of a multiclass linear discriminant classifier using the neuronal activities for all stimuli presented in sham (*Left*) and SNI (*Right*) animals. All on-diagonal values were significantly different from the off-diagonal stimuli within the same row ($P < 0.05$). (*O*, *Left*) bar graph of classification decoding accuracy for data in *N*. $^{**}P < 0.01$, unpaired *t* test. Sham, n = 14; SNI = 11 sessions. (*Right*) bar graph of misclassification cost of mistaking touch as painful. $^{*}P < 0.05$ unpaired *t* test sham, n = 50; SNI = 34 combinations. Data are presented as mean ± SEM.

and spurious nociceptive ensemble showed increased spontaneous activity, while nonresponding cells showed no difference (*SI Appendix*, Fig. S7). Moreover, we analyzed the resting-state functional neuronal connectivity at the population level using undirected graph theoretical analysis. In this way, the relational interplay between neurons can be characterized by two main variables: i) betweenness centrality, a

measure of the weighted number of shortest paths that pass through a given node (i.e., neuron), providing a measure of the relevance of that neuron in the passage of information throughout the overall neuronal network, and ii) degree centrality, a measure of the number of edges attached to a given node, indicating its connectivity level within the network. We found that while degree centrality was unaltered, betweenness centrality was significantly higher in the neuropathic pain condition (Fig. 3 *G* and *H* and *SI Appendix*, Fig. S8). This might suggest that neuropathic pain increased signal transfer between neurons in the ACC, contributing to the altered spontaneous activity. Besides, we found that the information, derived from Shannon's entropy, which is a measure of the structure of the neuronal activity patterns, was decreased in neuropathic pain, suggesting a degradation of information processing (Fig. 3*K*).

In terms of evoked responses, the turnover rate of sensory stimulus representation (i.e., stability) together with the selectivity and responsiveness was also highly dynamic and maintained in the neuropathic pain condition (*SI Appendix*, Fig. S9). The change in stimulus representation of a cell from one session to the other was not reflected in a change in its spontaneous activity. Additionally, the number of neurons modulated by sensory stimuli and the proportion of supramodal neurons remained unchanged, while the size of the spurious nociceptive ensemble continued to remain at chance level (Fig. 3 *I* and *J* and *SI Appendix*, Fig. S3*F*). However, in neuropathic pain animals, the touch-evoked activity of supramodal neurons was significantly higher but not in touch-selective cells (Fig. 3 *L* and *M*). Overall, the supramodal ensemble was more excitable in SNI as compared to sham, showing higher average activation to noxious and non-noxious stimuli (*SI Appendix*, Fig. S10). Altogether, these findings posit that these multifaceted cells might be candidates to represent nociceptive hypersensitivity in the ACC.

Our results so far suggest that the overall alterations in neuropathic pain affected excitability, network structure, and ensemble responses, which could have an impact on the population stimulus encoding in the ACC. These alterations could manifest themselves in an increased similarity of intrinsic stimulus-evoked activity patterns between noxious and non-noxious stimuli. Accordingly, in neuropathic pain the neuronal population activity patterns of innocuous stimuli became more equal to those of the noxious representation (*SI Appendix*, Fig. S11*A*). Furthermore, the similarity measured as mutual information within the supramodal neuronal ensemble responding to touch and noxious stimuli was higher in SNI as compared to sham (*SI Appendix*, Fig. S11 *B* and *C*). To test whether the increased similarity contributed to an error in stimulus classification, we assessed the correct decoding of individual stimuli in neuropathic and sham animals. Whereas all stimuli were properly discriminated in sham, there was a decrease in decoding accuracy and an increase in false classification (i.e., misclassification cost) of innocuous as noxious stimuli in neuropathic pain animals (Fig. 3 *N* and *O*).

Altogether, our data demonstrated profound changes in sensory encoding and inherent features of the ACC neuronal population in neuropathic pain due to defective neuronal activity and connectivity at the network level, which lead to an abnormal representation of nociceptive attributes. This accumulated in an aberrant encoding of the ACC nociceptive sensory space, contributing to a "blurred" sensory representation during neuropathic pain (35).

Analgesic Treatment Restores Sensory Coding. If neuropathic pain manifests itself as a faulty pattern separation by ACC neuronal ensembles, pain relief might restore the ability of these networks to discriminate between sensory inputs. We tested the plausibility of this assumption with GBP, which is a clinically relevant analgesic and represents the first line of defense to treat neuropathic pain symptoms (35). A single subcutaneous injection of GBP (s.c., 25 mg/kg) caused a long-lasting antihyperalgesic effect in neuropathic animals without apparent side effects (Fig. 4 *A* and *C* and *SI Appendix*, Fig. S12). Furthermore, GBP treatment reduced the manifestation of affective/motivational behavioral responses to nociceptive sensory stimuli (Fig. 4*D* and *SI Appendix*, Fig. S14*B*). Subsequently, we tested the stimulus representation in sham and neuropathic pain animals in the analgesic state. Contrary to what we expected, GBP increased the spontaneous activity of ACC neurons in both conditions and it did not restore the stimulus-evoked responses of supramodal neurons in SNI animals resulting in a lack of correlation between neuronal activity and the affective behavioral outcome (*SI Appendix*, Fig. S13), indicating that the analgesic turned the ACC network into an altered functional state that was different from both the naïve and neuropathic pain condition.

Despite this, GBP restored decoding accuracy and decreased the failure rate of stimulus classification (Fig. 4 *E* and *F* and *SI Appendix*, Fig. S14*A*). In line with this, the differences in the stimulus-evoked neuronal activity patterns of innocuous stimuli to those of the noxious representation were also recovered (Fig. 4*G* and *SI Appendix*, Fig. S11*A*) as well as the maladapted network architecture as measured by the betweenness centrality (Fig. 4*H*). There was no significant correlation between the decoding performance of sensory stimuli and the manifestation of affective behaviors triggered by a tactile stimulus (*SI Appendix*, Fig. S14*C*) in SNI mice before and after treatment with GBP, suggesting that nociceptive stimulus representation and its behavioral outcome may be mediated by different neuronal populations. Our results therefore show that, although altered single-cell activity persisted, the abnormal encoding of stimuli in the ACC in neuropathic pain is partly recovered by analgesics, thus sharpening the sensory representation. This provides important new insights into the mode of action of drugs targeting neuropathic pain.

Discussion

Our longitudinal study of neuronal network dynamics revealed several novel key principles of nociceptive coding in the ACC, a brain region that is associated with processing of the emotional/affective component of pain (5–7). Overall, population coding is required for the selective representation of noxious, non-noxious aversive and neutral stimuli in the ACC. Furthermore, it allowed to predict the affective/motivational behaviors in freely moving neuropathic animals. Thus, the ACC is well informed about peripheral sensory stimulation in terms of modality and quality contributing to the appropriate behavioral response (6, 7). So far it was elusive whether selective patterns of activity in the ACC could distinguish noxious from other sensory stimuli with similar valence (3, 36, 37). We now revealed that the nociceptive experience and also its quality (e.g., burning for noxious heat and stabbing for pinprick) can be achieved by a combination of stimulus-selective neurons and supramodal neurons. This ensemble then can code for higher-order, generalized and abstract features or concepts of the nociceptive experience. So the corresponding experience of pain is based on a population code, but not on nocicption-specific neurons (2, 35, 36). Thus, we provide a cellular and network explanation for the long-standing idea based on human studies indicating that pain can be seen as a response to suprathreshold salient stimuli which evoke an arousal response and an attentional shift towards the stimulus (38). It remains to be shown how this neural representation of nociception is connected to the perceptual discrimination of sensory stimuli.

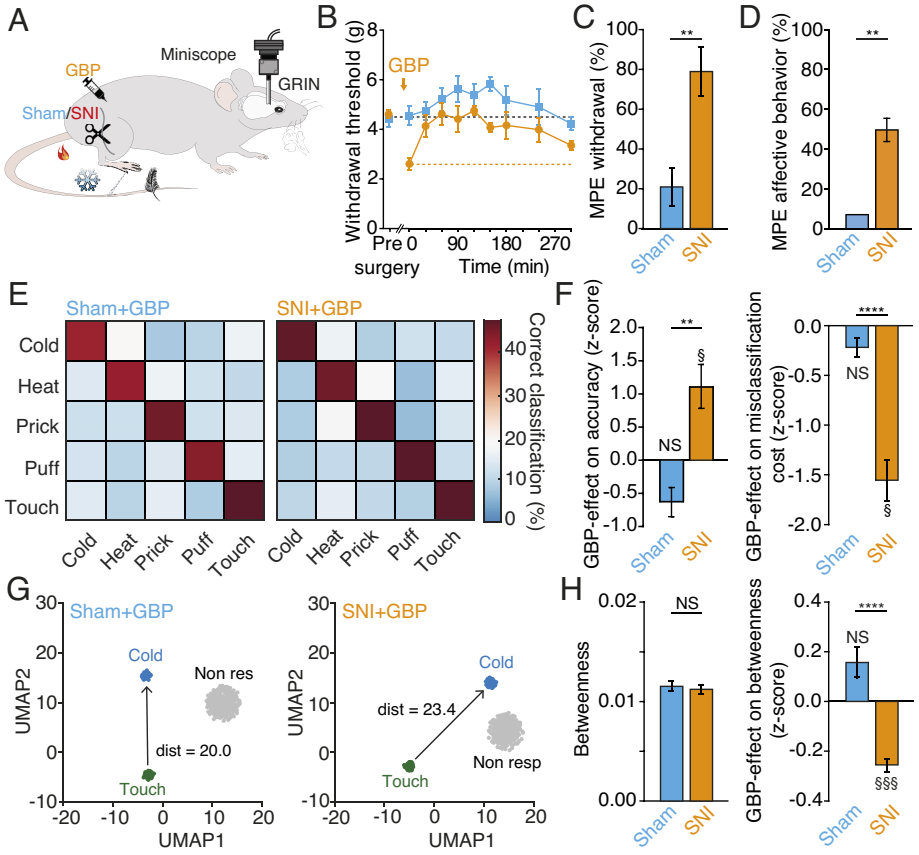

Fig. 4. Gabapentin restores stimulus representation in the ACC of neuropathic pain animals. (*A*) Sketch depicting the experimental condition. (*B*) Time course of the mechanical paw withdrawal threshold after a single injection of gabapentin (GBP, s.c., 25 mg/kg) in sham (n = 4, light blue) and SNI (n = 4, orange) animals. Dashed black line indicates average presurgery paw withdrawal threshold. (*C*) Maximum possible effects (MPE) of GBP on the paw withdrawal threshold determined for the time interval between 60 to 180 min after drug injection. ANOVA followed by Bonferroni post-hoc test, $F(3,26) = 15.43$; ****$P < 0.0001$, n = 4 mice. (*D*) MPE of GBP on the reduction of stimulus-evoked affective behaviors. n = 6 per group, **$P < 0.01$, Mann–Whitney *U* test. (*E*) Confusion matrices from a multiclass linear discriminant classifier, decoding stimulus identities of cold, heat, pinprick, puff and touch from the corresponding activity patterns in sham+GBP and SNI+GBP. All on-diagonal values were significantly different from the off-diagonal stimuli within the same row ($P < 0.05$). (*F*) Bar graph of net effect of GBP (z-scored relative to pre-GBP) on classification decoding accuracy (*Left*) or misclassification cost of touch as being noxious (*Right*). (*Left*) n = 6 per group; (*Right*) n = 50 per sham and n = 34 per SNI. NS, $P > 0.05$, *$P < 0.05$, ****$P < 0.0001$, Wilcoxon Signed Rank Test against 0. (*G*) Clustering of neurons (dots) based on the poststimulus response using UMAP for Sham+GBP and SNI+GBP. Note that the decreased distance between noxious cold and touch in SNI is reversed by GBP. Colors correspond to the favorable responsiveness of each neuron. (*H*) Graph-theoretic functional connectivity analysis of spontaneous neuronal Ca^{2+} activity in the ACC. (*Left*) quantification of betweenness for Sham+GBP against SNI+GBP. NS $P > 0.05$, unpaired *t* test. (*Right*) Net effect of GBP relative to pre-GBP state (z-score). NS, $P > 0.05$; ****$P < 0.0001$, Wilcoxon Signed Rank Test against 0. Sham+GBP, n = 310; SNI+GBP = 417 neurons.

The dynamic reconfiguration of the stimulus responsiveness and supramodality that we observed across sessions furthermore emphasize the lack of the existence of hard-wired stimulus-selective neurons. This may differ from neurons in the amygdala that keep responding to noxious stimuli over several weeks (39). Nevertheless, stable stimulus representation in the ACC at the population level is achieved by homeostatic principles that maintain the proportion of neurons responding, their responsiveness and reliability. In this way, the brain can achieve stability with a high degree of flexibility (31, 32). Since the ACC is not specific for pain (3), its function in nociception can be considered as a particular case of signaling the saliency value or uncertainty of an event to solve problems, recognize errors, control emotions and adapt responses according to ever-changing conditions (40, 41).

The development of chronic pain is associated with multiple cellular plasticity mechanisms within the pain processing system (42–45). On the level of the ACC, changes in neuronal excitability, synaptic plasticity, and alterations in the connectivity pattern have been described that might explain the phenotype (19, 21, 46). Nevertheless, it was not clear how such cellular changes would influence neuronal activity and coding capabilities on the circuit and ensemble level. Our data indicate that neuropathic pain results in increased spontaneous activity and stimulus-evoked responses in a supramodal ensemble that represents the intersect between innocuous and noxious stimuli. Furthermore, neuropathic pain was also associated with abnormal network connectivity, increased similarity of stimuli in the response activity space of noxious and innocuous representations resulting in a degradation of the decoding efficiency, and a misclassification of sensory stimuli. It is tempting to argue that the abnormal reactivity of supramodal neurons encodes the allodynic and emotional/affective component in the chronic pain condition (39). This would be consistent with the prevalent view that activity in the ACC is correlated to pain threshold (18). However, the fact that systemic administration of the analgesic GBP reversed sensory and affective consequences of neuropathic pain without restoring the spontaneous and stimulus-evoked activity of supramodal neurons challenges this interpretation and suggests that the common notion of hyperexcitability of neurons as a biomarker of chronic pain might not be predictive in all cases.

In this regard, it is important to consider the multiple cellular actions of gabapentinoids, which are thought to result in a reduction of neuronal excitability and transmitter release. Nevertheless, the overall effect on cortical neuronal circuits is still elusive. The network action observed in our study seem paradoxical as increased activity

in the ACC is considered as a hallmark of the chronic pain condition (19–23). It is therefore generally assumed that analgesics exert their effect by reducing neuronal activity, which has been suggested to be the mode of action of GBP in the spinal cord, periaqueductal grey and thalamus (42–44). The paradoxical increased excitability of the ACC, on the other hand, could not only activate descending modulatory pathways but also generate a rewarding signal that target mainly the affective/emotional component of pain (45, 46). Thus, this increased network activity could present a novel functional network state that promotes a decrease in uncertainty of stimulus identity (confusing a non-noxious stimulus as being noxious), which is transmitted to other cortical and subcortical areas of the pain matrix and in this way contributes to alleviate the painful sensation. Accordingly, GBP partially reversed the aberrant network architecture and sensory misclassification by the neuronal ensembles, implying that the disruption of sensory coding in the ACC is one of the mechanisms contributing to the chronic pain state. Therefore, it seems that GBP restores sensory accuracy through a modulation of the disturbed activity patterns. This was evident by the increase in distance in activity space, i.e. the activity patterns became more separated, improving classification performance. Our data revealed an inverse U-shaped relation between the affective pain behavior and the stimulus-evoked activity to touch, suggesting an optimal activity level in the chronic pain state to trigger affective behaviors, presumably due to the evoked unpleasantness. Increasing or decreasing the activity from this point alleviates the affective/emotional aspect of pain. This suggests that a cortical neuronal network in the pain matrix is designed to make a transition to an altered state after injury to optimally respond to pain.

Nevertheless, it remains to be shown in which way these overall changes are instrumental to the manifestation of the pathological affective pain state. The lack of correlation between the decoding performance of the stimulus-evoked activity and the affective behavioral responses in the different conditions, but the capacity to decode the behavior from the overall activity of the neuronal network in the ACC support the idea that different neuronal populations might mediate the nociceptive representation vs. its behavioral outcome (47). This transformation from input to output has yet to be determined. Nevertheless, the described changes are consistent with the concept of "sensory blurring" by chronic pain and "sensory sharpening" leading to analgesia that was observed in the somatosensory cortex of chronic pain patients (34). Thus, the hallmark of chronic pain at the neuronal network level is an aberrant network structure, exacerbation of responses to innocuous stimuli and an impairment of pattern separation and classification, providing a novel view on altered pain processing in the brain.

Summary of Materials and Methods

Animals. All experiments were conducted in accordance with the rules of the veterinary office of the canton of Bern, Switzerland. Male C57/BL6 mice (Central Animal Facility of the University of Bern or Janvier Labs, France) were housed in groups of 4 to 5 per cage and maintained on a 12-h light/dark cycle in a temperature-controlled environment with ad libitum access to food and water.

Surgeries. Adeno-associated viral particles carrying the genetically encoded calcium indicator GCaMP6f (ssAAV1/2.mCaMKIIa.GCaMP6f.WPRE.SV40(A); mCaMKIIa promotor-1288; titer: 6.2 × 10E12 vg/ml before dilution) were injected in the ACC (coordinates in mm: 0.75 AP, 0.4 ML, and −1.75 DV from Bregma). Seven to fourteen days after virus injection, GRIN lenses were implanted at coordinates: 0.75 AP, 0.4 ML, and −1.5 DV from Bregma. For the evaluation of neuropathic pain, the SNI model was used, where the sural nerve branch was left intact, while the peroneal and tibial nerve branches of the left sciatic nerve were ligated and cut.

Calcium Imaging Analysis. Two to three weeks after GRIN lens implantation, a baseplate for a miniaturized microendoscope (miniscope) was mounted. A total of six consecutive sessions, 1 wk apart, were recorded. Image registration was done with Turboreg (miniscope) in the MATLAB environment. After performing field-of-view (FOV) alignment with a custom-made graphical user interface (GUI), regions of interest were manually identified and segmented. Fluorescent calcium traces were extracted and normalized (as $\Delta F/F_0$) using a running-window average and calcium event-related spikes were inferred using the OASIS toolbox in MATLAB.

Spontaneous neuronal activity (resting-state activity) was measured when animals were undisturbed for 10 min before each stimulation session. The activity of each neuron was estimated by calculating the area under the curve (AUC) of the $\Delta F/F$ trace.

Stimulus-Evoked Responses. Animals were subjected to five stimuli, namely noxious cold, noxious heat, noxious pinprick, facial aversive air puff, and innocuous dynamic pain brush. Cold, pinprick and touch were applied to the plantar surface of the left hind paw (ipsilateral to the operated leg, contralateral to the imaged ACC region). Heat was applied to the proximal portion of the mouse's tail. Air puff was applied to either side of the animal's face. Each stimulus was presented at least 15 times, in blocks of three stimulations in a pseudo-random manner.

In order to determine stimulus-responsive neurons, we used a logistic regression classifier. We binned the inferred spikes and evaluated significant activations by comparing the trial-by-trial neuronal activity to a bootstrapped distribution. Responsiveness was evaluated based on the value of the Precision/Recall curve given by the classifier. Reliability was described as the number of significant trials over the total number of trials per session for a given stimulus.

Stimulus-evoked responses were evaluated by calculating the integral value (AUC) of the poststimulus evoked $\Delta F/F$ trace. Data was pooled across trials and animals.

Stimulus-Response Ensemble Categorization. All neurons were classified according to its significant response to the set of stimuli tested. Multimodal neurons were classified by being responsive to two or more stimuli. Within the multimodal ensemble, supramodal neurons were identified as neurons responding to a noxious stimulus and a non-noxious stimulus. The nociceptive ensemble was categorized as responding exclusively to two or more noxious stimuli, with no significant modulation by any non-noxious stimulus. The proportions obtained for each category were compared to a chance distribution obtained by 1,000 simulated response matrices by shuffling the identity of the responsive and nonresponsive cells keeping constant the proportion of responsive neurons.

Stimulus Decoding. We conducted multiclass linear discriminant classification to decode stimulus representation, using the inferred spikes per session and per animal. Data were then pooled to conduct statistics. We evaluated the accuracy of the decoder as well as the Matthew's correlation coefficient (MCC).

Behavior Decoding. We assessed the correct classification in neuropathic pain animals of two groups of behavioral outcomes (namely, affective-motivational behaviors and nonaffective but stimulus-oriented behaviors) together with no behavioral outcome based on population neuronal activity derived from the inferred

spikes, using a linear discriminant classifier. Behavioral labels were shuffled to calculate chance levels of decoding.

Clustering. Neurons responding to a pair of stimuli were pooled across animals and sessions. We then used the Uniform Manifold Approximation and Projection (UMAP) algorithm to reduce dimensions in the responsiveness of neurons. Centroids were obtained by k-mean clustering. The distance of each centroid in the UMAP space was measured.

Shannon's Entropy. Using bins of inferred spikes during resting-state spontaneous activity, we calculated the Shannon's entropy index by the bias-corrected Nemenman–Shaffe–Bialek estimation method.

Graph Theory. The inferred neuronal activity data acquired during resting-state spontaneous activity was used to evaluate the undirected graph by first computing the cross-correlation of neuronal activity. The adjacency matrix from the significant correlations using Monte Carlo simulations was calculated, and the normalized betweenness centrality, normalized degree centrality and normalized closeness centrality were evaluated per session, per animal. Additionally, the global network density was evaluated.

Effects of GBP (s.c., 25 mg/kg) on Neuronal Activity. In a different cohort of animals, 3 to 4 wk after SNI/sham surgery the maximumpossible effect, as well as GBP-related side effects, were evaluated. Once the optimal analgesic window was established (60 to 180 min post injection), 28 and 35 d after surgery (sham or NP), animals implanted with GRIN lenses and baseplates were subcutaneously injected with GBP and were subjected to the same imaging protocol as above.

Behavioral Assessments of GBP-Related Side Effects. To evaluate GBP-related side effects, motor coordination, muscle strength and sedation were tested in the rotarod test, horizontal wire test and the open field test, 3 to 4 wk after SNI surgery, 60 min post injection.

Data, Materials, and Software Availability. All study data are included in the article and/or *SI Appendix*. Our custom-designed MATLAB pipeline implementation for mySQL database registering, calcium imaging preprocessing, image registration, multiple-session segmentation GUI, activity trace extraction, deconvolution of calcium fluorescence, and animal behavior tracking are publicly available at our Gitlab website (https://gitlab.com/nevian_group_unibe/ca_imaging_data_analysis) (48). Additionally, all the third-party, open-source codes are also provided.

ACKNOWLEDGMENTS. We thank Natalie Nevian at University of Bern for her excellent technical assistance. Special thanks to Benjamin Grewe at the Institute of Neuroinformatics, ETH Zürich, for his initial help in setting up the miniscopes. We would also like to thank Christian Dellenbach, Jürk Burkhalter and Stefan Von Känel at the Department of Physiology, University of Bern for their skilled electronic, mechanical and IT support. This work was supported by the Swiss NSF (T.N., grant 159872; F.K. and T.N. 173486) and the European Research Council (T.N., grant 682905). F.K. is funded by the Agency for the Promotion of Science and Technology, Argentina (PICT-2018-0835/PICT-2018-0003).

1. A. V. Apkarian, M. C. Bushnell, R. D. Treede, J. K. Zubieta, Human brain mechanisms of pain perception and regulation in health and disease. *Eur. J. Pain* **9**, 463–484 (2005).
2. A. Mouraux, A. Diukova, M. C. Lee, R. G. Wise, G. D. Iannetti, A multisensory investigation of the functional significance of the "pain matrix". *Neuroimage* **54**, 2237–2249 (2011).
3. T. D. Wager *et al.*, Pain in the ACC? *Proc. Natl. Acad. Sci. U.S.A.* **113**, E2474–E2475 (2016).
4. T. D. Wager *et al.*, An fMRI-based neurologic signature of physical pain. *N. Engl. J. Med.* **368**, 1388–1397 (2013).
5. P. Rainville, G. H. Duncan, D. D. Price, B. Carrier, M. C. Bushnell, Pain affect encoded in human anterior cingulate but not somatosensory cortex. *Science* **277**, 968–971 (1997).
6. R. C. Coghill, C. N. Sang, J. M. Maisog, M. J. Iadarola, Pain intensity processing within the human brain: A bilateral, distributed mechanism. *J. Neurophysiol.* **82**, 1934–1943 (1999).
7. C. L. Kwan, A. P. Crawley, D. J. Mikulis, K. D. Davis, An fMRI study of the anterior cingulate cortex and surrounding medial wall activations evoked by noxious cutaneous heat and cold stimuli. *Pain* **85**, 359–374 (2000).
8. E. L. Foltz, L. E. White Jr., Pain "relief" by frontal cingulumotomy. *J. Neurosurg.* **19**, 89–100 (1962).
9. J. P. Johansen, H. L. Fields, B. H. Manning, The affective component of pain in rodents: Direct evidence for a contribution of the anterior cingulate cortex. *Proc. Natl. Acad. Sci. U.S.A.* **98**, 8077–8082 (2001).
10. J. P. Johansen, H. L. Fields, Glutamatergic activation of anterior cingulate cortex produces an aversive teaching signal. *Nat. Neurosci.* **7**, 398–403 (2004).
11. P. N. Fuchs, Y. B. Peng, J. A. Boyette-Davis, M. L. Uhelski, The anterior cingulate cortex and pain processing. *Front. Integr. Neurosci.* **8**, 35 (2014).
12. Q. Zhang *et al.*, Chronic pain induces generalized enhancement of aversion. *Elife* **6**, e25302 (2017).
13. R. W. Sikes, B. A. Vogt, Nociceptive neurons in area 24 of rabbit cingulate cortex. *J. Neurophysiol.* **68**, 1720–1732 (1992).
14. T. Koyama, K. Kato, Y. Z. Tanaka, A. Mikami, Anterior cingulate activity during pain-avoidance and reward tasks in monkeys. *Neurosci. Res.* **39**, 421–430 (2001).
15. K. Iwata *et al.*, Anterior cingulate cortical neuronal activity during perception of noxious thermal stimuli in monkeys. *J. Neurophysiol.* **94**, 1980–1991 (2005).
16. H. Mertz *et al.*, Regional cerebral activation in irritable bowel syndrome and control subjects with painful and nonpainful rectal distention. *Gastroenterology* **118**, 842–848 (2000).
17. R. H. Gracely, F. Petzke, J. M. Wolf, D. J. Clauw, Functional magnetic resonance imaging evidence of augmented pain processing in fibromyalgia. *Arthritis Rheum.* **46**, 1333–1343 (2002).
18. K. B. Jensen *et al.*, Brain activations during pain: A neuroimaging meta-analysis of patients with pain and healthy controls. *Pain* **157**, 1279–1286 (2016).
19. S. M. Blom, J. P. Pfister, M. Santello, W. Senn, T. Nevian, Nerve injury-induced neuropathic pain causes disinhibition of the anterior cingulate cortex. *J. Neurosci.* **34**, 5754–5764 (2014).
20. M. Santello, T. Nevian, Dysfunction of cortical dendritic integration in neuropathic pain reversed by serotoninergic neuromodulation. *Neuron* **86**, 233–246 (2015).
21. T. V. Bliss, G. L. Collingridge, B. K. Kaang, M. Zhuo, Synaptic plasticity in the anterior cingulate cortex in acute and chronic pain. *Nat. Rev. Neurosci.* **17**, 485–496 (2016).
22. F. Kasanetz, T. Nevian, Increased burst coding in deep layers of the ventral anterior cingulate cortex during neuropathic pain. *Sci. Rep.* **11**, 24240 (2021).
23. N. Hogrefe *et al.*, Long-lasting, pathway-specific impairment of a novel form of spike-timing-dependent long-term depression by neuropathic pain in the anterior cingulate cortex. *J. Neurosci.* **42**, 2166–2179 (2022).
24. U. Marti Mengual *et al.*, Efficient low-pass dendro-somatic coupling in the apical dendrite of layer 5 pyramidal neurons in the anterior cingulate cortex. *J. Neurosci.* **40**, 8799–8815 (2020).
25. A. S. Tolias *et al.*, Recording chronically from the same neurons in awake, behaving primates. *J. Neurophysiol.* **98**, 3780–3790 (2007).
26. M. L. Andermann, A. M. Kerlin, R. C. Reid, Chronic cellular imaging of mouse visual cortex during operant behavior and passive viewing. *Front. Cell. Neurosci.* **4**, 3 (2010).
27. S. P. Peron, J. Freeman, V. Iyer, C. Guo, K. Svoboda, A cellular resolution map of barrel cortex activity during tactile behavior. *Neuron* **86**, 783–799 (2015).
28. J. Poort *et al.*, Learning enhances sensory and multiple non-sensory representations in primary visual cortex. *Neuron* **86**, 1478–1490 (2015).
29. T. Rose, J. Jaepel, M. Hubener, T. Bonhoeffer, Cell-specific restoration of stimulus preference after monocular deprivation in the visual cortex. *Science* **352**, 1319–1322 (2016).
30. L. N. Driscoll, N. L. Pettit, M. Minderer, S. N. Chettih, C. D. Harvey, Dynamic reorganization of neuronal activity patterns in parietal cortex. *Cell* **170**, 986–999.e16 (2017).
31. M. E. Rule *et al.*, Stable task information from an unstable neural population. *Elife* **9**, e51121 (2020).
32. C. Johnson *et al.*, Highly unstable heterogeneous representations in VIP interneurons of the anterior cingulate cortex. *Mol. Psychiatry* **27**, 2602–2618 (2022).
33. A. Li *et al.*, Disrupted population coding in the prefrontal cortex underlies pain aversion. *Cell Rep.* **37**, 109978 (2021).
34. C. Clopath, T. Bonhoeffer, M. Hubener, T. Rose, Variance and invariance of neuronal long-term representations. *Philos. Trans. R. Soc. Lond. B Biol. Sci.* **372**, 20160161 (2017).
35. P. Haggard, G. D. Iannetti, M. R. Longo, Spatial sensory organization and body representation in pain perception. *Curr. Biol.* **23**, R164–R176 (2013).
36. G. D. Iannetti, A. Mouraux, From the neuromatrix to the pain matrix (and back). *Exp. Brain Res.* **205**, 1–12 (2010).
37. T. D. Wager, L. Y. Atlas, How is pain influenced by cognition? Neuroimaging weighs in. *Perspect. Psychol. Sci.* **8**, 91–97 (2013).
38. V. Legrain, G. D. Iannetti, L. Plaghki, A. Mouraux, The pain matrix reloaded: A salience detection system for the body. *Prog. Neurobiol.* **93**, 111–124 (2011).
39. G. Corder, *et al.*, An amygdalar neural ensemble that encodes the unpleasantness of pain. *Science* **363**, 276–281 (2019).
40. B. A. Vogt, Pain and emotion interactions in subregions of the cingulate gyrus. *Nat. Rev. Neurosci.* **6**, 533–544 (2005).
41. I. E. Monosov, Anterior cingulate is a source of valence-specific information about value and uncertainty. *Nat. Commun.* **8**, 134 (2017).
42. V. K. Samineni, L. S. Premkumar, C. L. Faingold, Neuropathic pain-induced enhancement of spontaneous and pain-evoked neuronal activity in the periaqueductal gray that is attenuated by gabapentin. *Pain* **158**, 1241–1253 (2017).
43. M. Russo, B. Graham, D. M. Santarelli, Gabapentin-friend or foe? *Pain Pract.* **23**, 63–69 (2023).
44. R. Patel, A. H. Dickenson, Neuronal hyperexcitability in the ventral posterior thalamus of neuropathic rats: Modality selective effects of pregabalin. *J. Neurophysiol.* **116**, 159–170 (2016).
45. K. Bannister *et al.*, Multiple sites and actions of gabapentin-induced relief of ongoing experimental neuropathic pain. *Pain* **158**, 2386–2395 (2017).
46. K. Hayashida, H. Obata, K. Nakajima, J. C. Eisenach, Gabapentin acts within the locus coeruleus to alleviate neuropathic pain. *Anesthesiology* **109**, 1077–1084 (2008).
47. D. Jercog *et al.*, Dynamical prefrontal population coding during defensive behaviours. *Nature* **595**, 690–694 (2021).
48. M. A. Acuña, P. De Luna, T. Nevian, Calcium imaging data analysis. Gitlab. https://gitlab.com/nevian_group_unibe/ca_imaging_data_analysis. Deposited 8 December 2021.